ARMA 09-82

Estimating the Extent of the Disturbed Rock Zone around a WIPP Disposal Room

Herrick, C.G., Park, B.Y., and Lee, M.Y.
Sandia National Laboratories, Carlsbad, NM, USA
Holcomb, D.J.
Sandia National Laboratories, Albuquerque, NM, USA

This paper was prepared for presentation at Asheville 2009, the 43rd US Rock Mechanics Symposium and 4th U.S.-Canada Rock Mechanics Symposium, held in Asheville, NC June 28th – July 1, 2009.

ABSTRACT: The disturbed rock zone (DRZ) is an important feature which is evaluated in the Waste Isolation Pilot Plant (WIPP) performance assessment (PA) to predict post-closure repository performance. Mining of a WIPP disposal room disturbs the stress state sufficiently to cause fracturing of the surrounding rock, and this fracturing will alter the mechanical and hydrological properties of the salt. DRZ extent, and permeability, controls the majority of the brine that enters or exits the repository in PA modeling of the undisturbed scenario. Extensive laboratory data from experiments performed on rock salt demonstrate that damage can be modeled in terms of stress invariants. In this paper the DRZ extent is calculated based on a dilatant damage criterion. The calibrated damage factor *C* in the damage criterion is determined by comparing ultrasonic wave velocity field measurements obtained in the S-90 drift with a numerical analysis that predicts the salt's behavior. Ultrasonic velocities decrease in the presence of microcracks and loosened grain boundaries associated with salt damage. The most extensive DRZ exists during early times, within the first ten years of mining. The maximum predicted DRZ surrounding a WIPP disposal room is approximately 2.25 m below, 4.75 m above, and 2 m laterally. This paper also presents several lines of evidence, based on previous studies, that support the prediction of DRZ size by applying a WIPP specific damage criterion calibrated using ultrasonic velocity measurements.

1. INTRODUCTION

The Waste Isolation Pilot Plant (WIPP), located in southeastern New Mexico, is operated by the U.S. Department of Energy (DOE) as the underground disposal facility for defense-related transuranic (TRU) waste. It is located in the Salado bedded salt formation at a depth of about 655 m (Figure 1). Salt at this depth behaves as a viscous material having a stress state that is initially at lithostatic. Mining of the salt disturbs the static equilibrium and induces three deformational processes: (1) elastic deformation, (2) inelastic viscoplastic flow, and (3) inelastic-damage induced flow [1]. Fracturing of the rock surrounding a disposal room changes the mechanical and hydrological properties of the salt. The extent and permeability of this disturbed rock zone (DRZ) controls the majority of the brine that enters or leaves the repository under 'undisturbed' conditions (i.e., no human intrusion into the repository). As shown in Figure 1, Location 1 in the S-90 ("South 90") access drift to Room Q provided an opportunity to conduct geophysical investigations of the extent of salt damage for a nearly perfect two-dimensional configuration isolated from other areas of rock disturbance.

2. ULTRASONIC VELOCITY MEASUREMENTS

Inelastic-damage induced flow (or simply "damage"), which is manifested by the initiation, growth, coalescence, and healing of microfractures, is the least understood of the three deformational processes mentioned above. Over the years, various methods have been undertaken to measure the spatial and temporal changes during salt damage. This study used ultrasonic velocity measurements obtained from the rib (side) of the S-90 access drift, which was excavated in 1988, to assess the extent of the DRZ [2]. Brodsky [3] demonstrated in salt that changes in ultrasonic velocity can be related to damage due to microcracking.

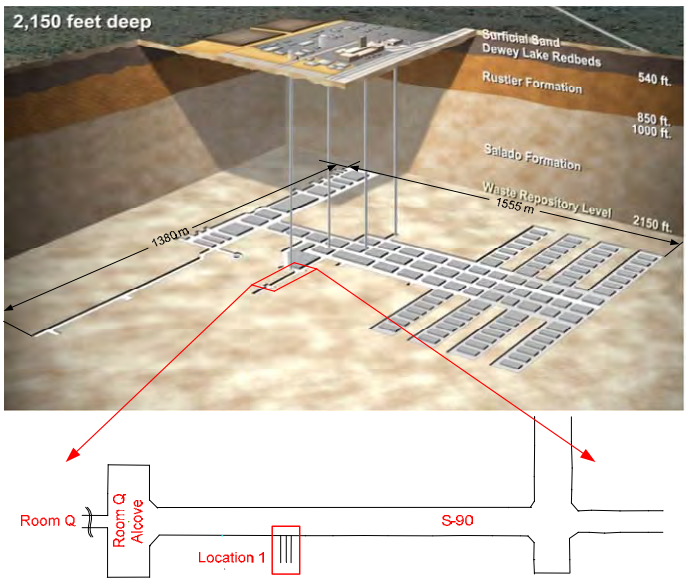

Figure 1. Schematic diagram of the WIPP repository. The expanded red-boxed area indicates the location where the underground tests were conducted (Location 1).

Ultrasonic wave velocities decrease in the presence of open cracks and loosened grain boundaries. The effect is strongest for cracks oriented perpendicular to the particle motion induced by the wave. Thus the extent of the disturbed zone can be determined by propagating ultrasonic waves through successive portions of the formation. Cracking responsible for the disturbed zone is expected to vary as a function of distance from the face of the rib and is dependent on the position of the measurement path relative to the back (roof) and floor. The undisturbed zone is defined as that region where the elastic wave speed remains constant with increasing depth from the rib. Measurements were made between pairs of holes ("cross-hole") cored perpendicular to the axis of the drift along horizontal and vertical paths lying in vertical planes parallel to the rib. Between each pair of holes, travel time measurements were made at 30 cm (1 ft) intervals to a depth of about 7 meters (~20 ft), as measured from the rib face. In addition, measurements were made within one hole ("same-hole") along paths perpendicular to the drift wall. The paths for the cross-hole measurements were nominally one meter long, while the same-hole measurements all had the a fixed path length of nominally 33 cm. Travel time measurements were made using the technique commonly used for ultrasonic sound velocity determination in rock. A sound pulse is applied to the rock at a known time and place and, after traveling through the rock, is received by a transducer at a known distance. *P*- (compression) wave velocity, V_P, and *S*- (shear) wave velocity, V_S, data were used for these measurements.

2.1. *Hole Layout and Lithology*

Nine holes were cored to sample the lithologies exposed in the access drift and to assess the stress state from top to bottom of the rib. As shown in Figure 2, the hole locations were chosen such that three map units were sampled, namely, the upper argillaceous halite, pure halite, and lower argillaceous; as well as the expected variation in damage along the height of the rib. Each hole was 10.16 cm (4 inches) in diameter, approximately 7 meters (~20 ft) deep, and as close to horizontal as possible. Great effort and care was taken by the surveying and drilling crews to align the holes parallel and horizontal. Hole-to-hole separation varied by less than 10 cm (~4 inches) over the depth, indicating very good control on the starting angle and carefully controlled drilling.

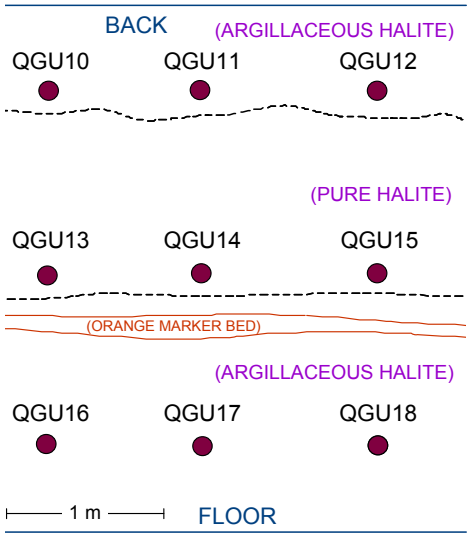

Figure 2. Borehole layout for ultrasonic velocity tests conducted at Location 1 in the S-90 drift. Borehole identification numbering: Q – Room Q alcove or access drift, G – geophysical, U – ultrasound / acoustic, 1 – borehole suite location 1, and 0 through 8 – borehole numbers.

Redundancy was added to the system by including a third column of holes (QGU12, QGU15 and QGU18). Measurements between QGU10 and QGU11 should be similar to the results observed between QGU11 and QGU12, with the exception of small-scale variations in the lithology due to fluctuations in the boundary between the map units.

2.2. *Measurement System*

Piezoelectric transducers were used as both the transmitter and receivers of the ultrasonic elastic waves. In the current work, only compressional mode transducers were used, although in certain configurations, a shear mode can be generated. A 300 kHz, PZT-5A piezoelectric disk was the basic element; four of these were used, two as transmitters and two as receivers. Each disk was mounted inside of a housing that could be pressed against the side of the boreholes using air pressure (Figure 3). Suitably-curved faces on the aluminum housing increased the area of contact when the housing was extended by pressurization to, typically, 0.4 MPa (60 psi). To further, and very

substantially, increase the energy transmission across the housing-rock interface, a couplant was extruded between the housing face and the rock. Corn syrup was used for this as it is inexpensive, cleans up easily, and provides good coupling for both compressional and shear elastic waves.

Two transducer housings were coupled together to form the tool inserted into the borehole (Figure 3). Each transducer was electrically independent, meaning that either could be driven and/or act as a receiver. One advantage of this approach is the ability to make two measurements at one tool position, thereby reducing the measurement time by eliminating the need to reposition the tool. An additional capability is gained by placing two transducers in one hole; one transducer can be driven as a transmitter while the other acts as a receiver. This allows measurements to be made along paths normal to the rib face and orthogonal to the cross-hole measurements. Since the orientation of the damage is expected to be anisotropic, additional information is gained by being able to measure the effects of damage along orthogonal paths. In particular, it is expected that the cracking planes will be preferentially parallel or sub-parallel to the rib, resulting in the largest changes in velocity along paths normal to the rib.

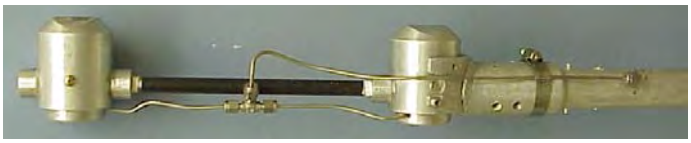

Figure 3. Photograph of one of the measurement tools showing the plumbing for couplant transport and pressurizing the air cylinders. Transducer separation is 30.5 cm (1 ft).

In addition to measurements of compressional mode (*P*) velocity, this technique allows the generation and propagation of shear (*S*) waves through the material parallel to the hole axis. All PZT-5 ceramic transducers expand and contract along the axis parallel to the direction of polarization when an electrical field is applied and generate an electrical field when an impinging mechanical disturbance causes strain along the axis of polarization. A disk of PZT-5, a so-called *P*-mode transducer, is polarized parallel to the axis of the disk; application of an electrical field results in the disk getting thicker or thinner, according to the sense of the electric field. When coupled mechanically to the surrounding medium, the rapid change in shape causes a wave to propagate into the rock in the direction parallel to the disk axis and the result is a *P*-wave where the particle motion is parallel to the propagation direction. However, at right angles to the disk axis, another disturbance propagates. In this case, the particle motion is still parallel to the disk axis, but the propagation direction is now orthogonal. This is a shear wave, characterized by particle motion perpendicular to the direction of propagation. Thus, a *P*-mode transducer can generate and detect *S*-waves, and this was done using the pair of transducers in a single hole.

Once positioned and pressurized, the chosen transducer was excited by a 100-volt square pulse, with a rise time of about 200 ns. The resulting wave was detected by the chosen receiver, amplified by 60 dB and recorded on a digital oscilloscope to 16-bit precision, at a sampling rate of 10 or 20 MHz. Each data set, consisting of the recorded driving pulse and received pulse, was transferred to computer storage for later analysis. To enhance signal quality, 100 signals were averaged at each position. For cross-hole measurements, only *P*-waves were recorded, with measurements made at 30 cm (1 foot) intervals from the full depth of the holes to the surface. Positioning was done by measuring the tool depth relative to surveyed marks on reference plate collars affixed at the hole's entrance because calculation of velocities requires an accurate knowledge of the transmitter and receiver positions.

2.3. Surveying

The goal was to determine wave speeds with an accuracy of plus or minus 0.5%. Path lengths ranged from about 1 meter for the cross-hole measurements to a fixed nominal 0.33 meters for the same-hole measurements. The wave speed for *P*-waves in salt is approximately 4500 m/sec for undisturbed salt. Thus travel times were expected to be in the range of 200 to 70 microseconds. To maintain the desired accuracy, the path length had to be known to a precision greater than 0.5%, or 5 mm, for the cross-hole paths. Since no direct measurement of path length was possible, the path had to be determined indirectly by determining the three-dimensional position of each transducer as a function of depth in the hole. A survey was conducted by Westinghouse to locate the center line of each of the measurement holes to an accuracy of plus or minus 1 mm, and a second survey achieved an even higher level of accuracy.

2.4. Data Analysis

Calculation of velocity is a multi-step process that involves determining the coordinates, correcting for various offsets, and identifying the arrival time for the *P* or *S* wave at the receiver. Coordinates were determined by parameterizing the North, East and vertical coordinates (N, E, and Z) of the surveyed center line of each hole as a function of depth in the hole. Three second-order fits for N, E, and Z as functions of depth were determined and found to reproduce the surveyed coordinates within the required degree of accuracy. For each measurement set, the measured depth of emplacement for the transducer was used in the second-order fits to calculate the coordinates of the transducer in space. Offsets were applied to account for the actual position of the transducer against the wall, instead of the centerline of the hole. Knowing the coordinates of the

transmitter and receiver, the path length could be calculated. Non-systematic errors are estimated to make the uncertainty in cross-hole path length be less than 3 mm.

To calculate the travel time, the difference between the time of the initiating electrical pulse applied to the transmitter and the time of arrival of the *P*- or *S*-wave at the receiver must be known. Pulse time, which is determined from the rising square wave, is known to an accuracy limited only by the typical sample interval of 50 or 100 ns, and thus, it contributed a negligible amount to uncertainty in velocity. It is much more difficult to fix the arrival time of the wave at the receiver. The waveform is an emergent sinusoid, not a square wave pulse, whose unsharp beginning is further obscured by electrical noise in the highly amplified signal. *S*-waves, which travel slower and arrive later than *P*-waves, are further obscured by the coda of the *P*-wave that extends into the *S*-wave signal.

Although signal quality was improved by signal averaging, the determination of arrival times could still be difficult especially for measurement paths that passed close to the surface where damage was greatest, resulting in high attenuation of the signal. Typically the first arrival is small in amplitude, making it easy to miss the first cycle or more in a highly attenuated signal. This would result in unacceptable errors in the travel time and velocity. Visual comparison of the signals in a given data set can be used to minimize the risk of missing first arrivals.

An interactive Matlab program has been developed that allows the signals from a given data set to be plotted and offset so that the arrival times are aligned. When arrival times are correctly chosen, the similarity of the signals is usually obvious. The program allows the arrival times to be adjusted interactively until the signal-to-signal correlation is good. For the measurement paths at some distance from the free surface the lower attenuation results in a more impulsive signal. As a result, the actual arrival time is easily determined, allowing these signals to be used as a guide for choosing the arrival time for the weaker, more emergent signals from paths near the free surface. Typically one clear arrival is used as a reference and all the other signals are adjusted to correlate well with that reference. This produces a systematic error corresponding to the error in the choice of the reference signal, but it reduces the scatter between measurements, making it much easier to see trends in the velocity with depth. This systematic error was less than 200 ns (~0.1%), a negligible amount for the cross-hole *P*-waves. Same-hole *P*-waves are much lower amplitude because of the unfavorable geometry of the transmitter and receiver. As a result, the errors are larger, and the effect is more significant due to the shorter path lengths. The systematic error is close to 1% for these paths, but of course, that is a constant error for all measurements. Trends are not obscured as a result.

Shear waves travel slower than *P*-waves and there is always energy emitted as *P*-waves. Thus, the *S*-wave arrival must be detected while the P wave is still influencing the transducer. Typically, a large, fairly sharp sinusoid emerging from the *P*-wave coda is taken as the *S*-wave arrival. The technique of comparing waveforms is essential to obtaining consistent results for *S*-waves because determining the actual arrival time is usually difficult. A reference signal with the sharpest *S*-arrival is chosen and a particular peak within the signal is used to align the other signals. Inevitably this introduces a systematic error of 1 or 2% in the *S*-velocity, but the trends are unaffected as the error applies to all the referenced signals.

2.5. Inferred DRZ Depth Measurements

The depths of DRZ are inferred from the ultrasonic wave velocity data measured at Location 1 (Figure 1). Measurements were made horizontally for all six cross-hole possibilities, vertically for four of six cross-hole possibilities, and perpendicular to the rib (same-hole) in four of the nine holes (Figure 2). All of the data analyses and plotting was performed by Holcomb and Hardy [2]. Plots contain a title giving the location data, the wave type (*P* or *S*), and the data plotted as the measured velocity plotted at the depth of the transmitter. As an example, Figure 4(a) shows the velocity data versus depth from cross-hole *P*-wave measurements between boreholes QGU14 (transmitter) and QGU15 (receiver). The velocity increases from a low of 3.84 km/s at 0.15 m depth to 4.61 km/s at 1.83 m depth. The velocity does not increase beyond 1.9 m depth, but exhibits variations around a constant value of 4.63 km/s. Figure 4(b) shows the velocity versus depth for a same-hole test in QGU14 using *S*-waves. The velocity increases from 1.04 km/s at 0.15 m depth to 2.73 km/s at 1.8 m. No systematic velocity variations were observed beyond 1.8 m, although there were variations about the best-fit value of 2.75 km/s.

A bilinear model was used to describe the velocity versus depth data (Figure 4). To develop the model parameters, a depth was chosen by inspection that marked the deepest extent of the DRZ. Then a line of the form $y = V_0$ was fit to the data points at depths greater than the deepest point of the DRZ and a line of the form $y = ax+b$ was fit to the data points at shallower depths. The fits were performed using the trend line capability in a commercially available spreadsheet application. The average velocity beyond the DRZ, V_0, is considered to be the wave velocity in the undisturbed salt. The intersection of the trend line $y = ax+b$ and the average value line can be regarded as an inferred DRZ depth. The inferred DRZ depths in Figures 4(a) and (b) are calculated as 1.719 m and 1.796 m, respectively.

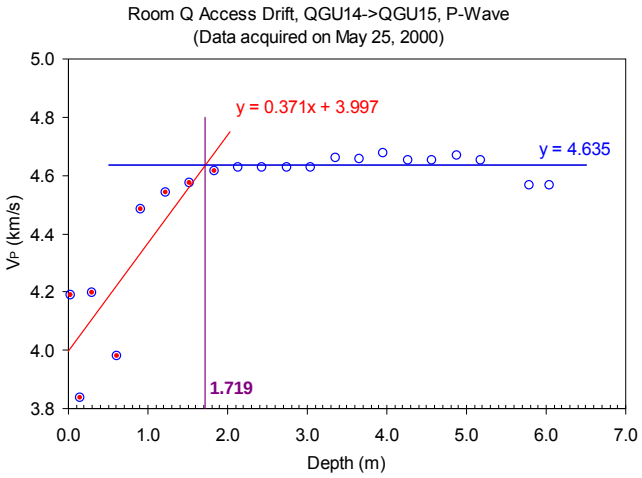

(a)

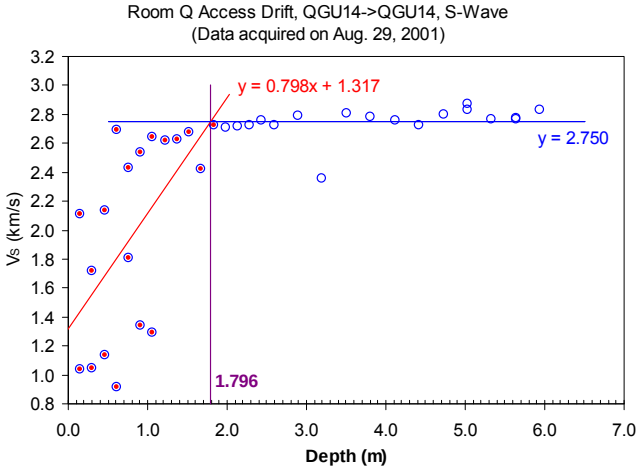

(b)

Figure 4. Velocity data versus depth with fitted linear trend and average lines from (a) cross-hole test between boreholes QGU14 (Transmitter) and QGU15 (Receiver) using *P*-waves, and (b) same-hole test in borehole QGU14 using *S*-waves. The fitted linear trend data are thought to be indicative of damaged rock and the constant line of the undisturbed intact salt.

3. ESTIMATING THE DRZ EXTENT

3.1. Dilatant Damage Criterion

Extensive laboratory salt creep data has demonstrated that a dilatant damage in salt can be modeled in terms of the ratio of stress invariants [4]:

$$D = \frac{C \cdot I_1}{\sqrt{J_2}} \qquad (1)$$

where D is the damage potential, I_1 is the first invariant of the stress tensor, and J_2 is the second invariant of the deviatoric stress tensor. When $D < 1$, the shear stresses in the salt (J_2) are large relative to the mean stress (I_1), and damage is predicted. The calibrated damage factor C is considered to be site-specific.

3.2. Structural Analysis of the S-90 *Drift*

A two-dimensional plane-strain model is used to represent the S-90 drift and surrounding rock [5]. The model grid (Figure 5) represents the cross-section of the drift in two dimensions. Invoking symmetry, only half of the drift is modeled. The drift is modeled as being subjected to regional far-field boundary conditions acting from an infinite distance away. The distance from the axis of the drift to the confining boundary is 50 m. This distance is about ten times the width of the drift. A lithostatic stress ($\sigma_x = \sigma_y = \sigma_z$) that varies with depth is used as the initial stress condition. Gravity forces are included.

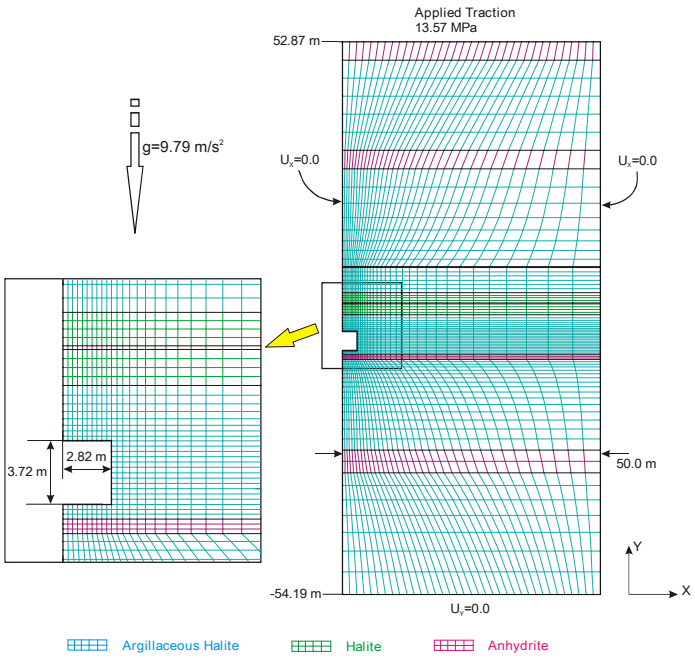

Figure 5. FEM mesh of the S-90 drift and imposed boundary conditions.

A zero-displacement boundary condition in the horizontal direction ($U_X = 0.0$) was applied on both the left and right boundaries of the model to represent the symmetric nature of the drift and far-field stresses, respectively. A prescribed normal traction of 13.57 MPa, corresponding to 603 m of overburden, was applied on the upper boundary and a vertical zero-displacement boundary condition ($U_Y = 0.0$) was applied on the lower boundary to react to the overburden load. Gas pressure, which results as a by-product of degradation and corrosion of the waste materials, is treated as a normal traction applied to the inner surface of the room. The initial half-symmetry drift dimensions are 3.72 m high by 2.82 m wide. The multimechanism deformation constitutive model was used to predict the rock salt creep behavior [6].

3.3. *Determination of the Calibrated Damage Factor C*

The change in DRZ extent with time is calculated by comparing the dilatant damage potential criterion with stresses determined by finite element analyses of the drift. Stresses in the salt are expected to change as a function of time due to salt creep, and the dimensions of the S-90 access drift began to decrease as soon as excavation was completed. Thus, knowledge of the time elapsed between completion of the excavation and the acquisition of the ultrasonic velocity data (12.3 and 13.7 years for the two sets of measurements) is necessary to estimate the value of the calibrated damage factor *C* in the dilatant damage criterion. The DRZ is created soon after the room is excavated when stress differences are relatively high and confining stresses are relatively low. The stress distribution changes over time because salt deforms plastically. This suggests that in the rib where the sonic data were collected, the damaging stress conditions may have existed deeper into the pillar at the early times than later, i.e. at the time the sonic velocity measurements were made. Therefore the stress conditions modeled at 12.3 and 13.7 years are not the same as the stress state that created the DRZ in the first place. However, due to the short time period between excavation of the drift and measurement of the ultrasonic velocities and the lack of an internal pressure on the inner boundary, the modeling suggests that this stress alteration has only a minor effect.

From the structural analysis of the drift, contours of the maximum extent of dilatancy damage around the drift can be drawn for different values of *C* using Equation 1. Each contour, therefore, represents a different potential for dilatancy damage to occur to the salt and is referred to as a dilatancy damage potential (DPOT) contour. Figure 6 shows the DPOT contours calculated at 12.3 years after excavation. Inferred DRZ depths determined by the method demonstrated in Figure 4 are also plotted on the figure as symbols. For simplicity since the differences between contour plots are small the DRZ depths at 12.3 and 13.7 years are all plotted in Figure 6 (see Park et al. [5] for full details of the analysis).

The DPOT contours correspond to different *C* values in Equation 1. A smaller value of *C* yields a greater extent of damage. The calibrated damage constant *C* for WIPP is determined from reading the contour values of DPOT corresponding to the inferred DRZ depths obtained from the ultrasonic velocity test data.

The average calibrated damage factor, *C*, in the dilatancy criterion was calculated to be 0.19 for the salt at the WIPP repository horizon. This *C* value represents the best estimate of the actual field value as it is based on a large number of controlled in situ measurements made in the S-90 drift. The constant *C* is assumed to be site specific and does not vary with time. It relates the magnitude of the deviatoric stresses to the mean stress at the onset of the creation of damage. It is assumed that the *C* value is uniform across the entire WIPP horizon due to the similar geology. However, the value of *C* may be different outside of this region.

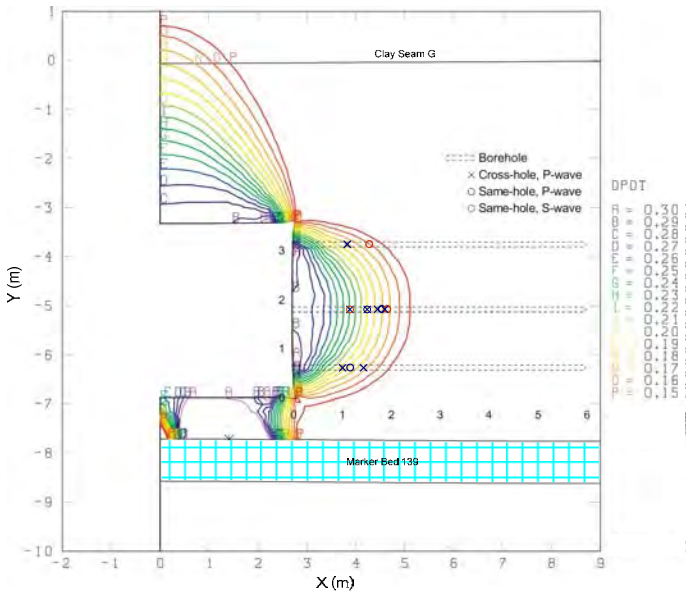

Figure 6. Comparison of DRZ depths determined from ultrasonic velocity measurements with DRZ extents predicted from FEM analyses using a range of *C* (DPOT) values.

3.4. *Determination of the Maximum DRZ Extent around a WIPP Disposal Room*

Assuming the WIPP-specific damage criterion $D = 0.19 I_1 / \sqrt{J_2}$ applies everywhere and the calibrated damage factor *C* does not vary with time, a modeled DRZ extent around a waste-filled room can be calculated using $D < 1$ for damaged salt and $D > 1$ for undisturbed salt. The results from previous structural analyses were used to determine the stress history surrounding WIPP disposal rooms for 10,000 years [7]. Thirteen different rates of gas generation were investigated in the previous study. The most critical stress condition leading to possible salt damage occurs almost immediately upon excavation, before any gases due to waste corrosion or degradation can be formed, before salt creep has relieved the stresses, and/or before the contacted waste produces a back stress. The calculated DRZ extent at this time according to Equation 1 will be at its greatest. The maximum calculated DRZ extent below and above a disposal room are approximately 2.25 m and 4.75 m, respectively (Figure 7), and the maximum lateral DRZ extent in the side of the room is roughly 2 m. The anhydrite layers, Anhydrite A and Marker Bed 139, act as a buffer against further DRZ propagation.

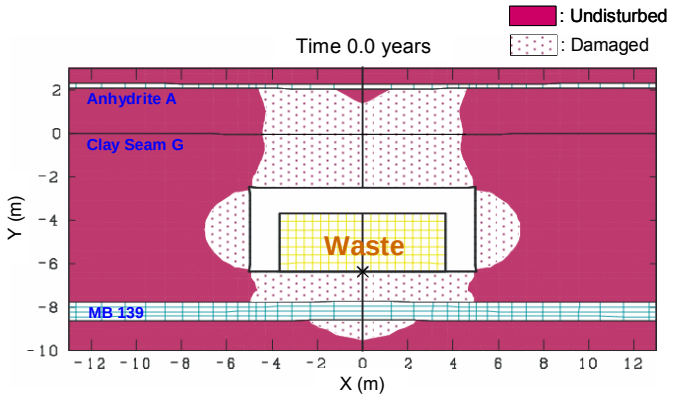

Figure 7. The calculated maximum extent of the DRZ around a disposal room.

4. COMPARISON OF THE ESTIMATED DRZ EXTENT WITH OTHER INDICATORS

Several lines of evidence from previous studies support calculation of the DRZ extent around a WIPP disposal room in the manner described in this paper. These studies will be discussed in this section.

Stormont [8] summarizes the results of 172 (nitrogen) gas permeability measurements made at numerous places in the WIPP horizon to identify regions within the rock salt which have experienced disturbance or damage. The gas permeabilities are given with respect to the effective radius of the excavation ($r = \sqrt{A/\pi}$, A = excavation area). Because of the variety of test geometries used to develop the above formula, its direct application is not always possible. However, Stormont does give a specific case (Room D) to which these results may be compared. He found that "beyond a certain depth (about 0.6*r*), the gas permeability is immeasurably small," i.e. less than 10^{-21} m^2. Converting into the DRZ extent of the S-90 drift yields a DRZ depth of 1.5 m; 0.2 m less than the average predicted in the current model (Figure 8). Stormont's measurement corresponds to C = 0.20.

Microstructural analysis performed on core taken from the central borehole (QGU14, Figure 2) revealed that the distribution of fractures is higher and the apertures of fractures are wider close to the rib face [9]. Of the 168 fractures measured in QGU14 core, only eight fractures at a depth of greater than 2 m have a measured aperture wider than 50 μm (Figure 9). Of those eight, only three fractures are greater than 100 μm and two of those are from an area of known coring damage. When compared with Stormont's results [8], it appears that only fractures with an aperture greater than 100 μm contribute to a measurable in situ gas permeability. Of the total QGU14 core fracture width measurements, 98-99% of the fractures with an aperture greater than 100 μm are within 1.8 m of the rib face. This correlates to C = 0.18.

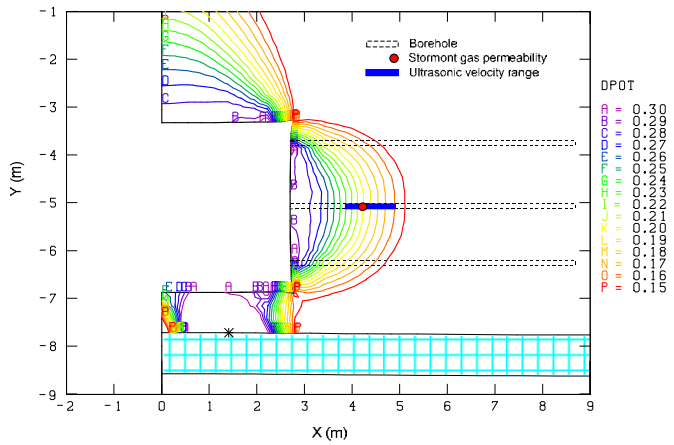

Figure 8. Comparison of the calculated DRZ extent based on Stormont (1997) in situ gas permeability results and ultrasonic velocity measurement range.

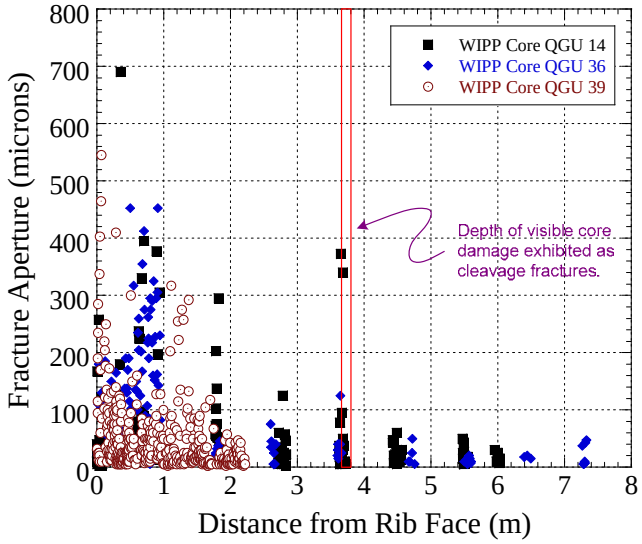

Figure 9. Plot showing the distribution of fractures and fracture apertures in three WIPP cores. Borehole QGU14 was used for ultrasonic velocity testing.

Van Sambeek et al. [4] examined laboratory triaxial compression tests that resulted in dilation of rock salt. They presented their results in terms of stress invariants I_1 and J_2. Their plot shows a clear linear delineation between those stress conditions that cause dilation and those that do not. This relationship was calibrated to fit our ultrasonic field data. In further laboratory triaxial compression and extension testing of bedded rock salt DeVries et al. [10] found an average value of C = 0.197 (Figure 10). This is in very good agreement with the field calibrated damage factor in this study. DeVries et al. [10] also showed that salt damage appears to be loading path dependent.

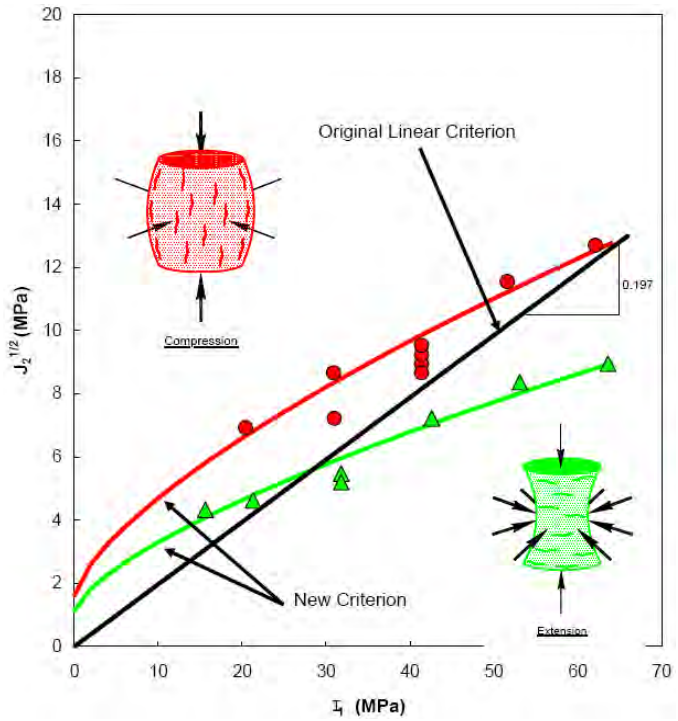

Figure 10. A copy of Figure 10 from DeVries et al. [10] showing that if the results of their laboratory test results were cast into the original linear criterion [4], a *C* value of 0.197 would be obtained.

5. CONCLUSIONS

Excavation of a disposal room in rock salt creates a stress state that induces fracture. This disturbance is manifested by dilation of formerly competent rock, altering its intact properties. The creation, evolution, and engineering properties of the DRZ influence the WIPP's performance during operations and after closure. Characteristics of the DRZ are important in the assessment of post-closure repository performance due to its control over brine flow into and out of the repository in the analysis of the undisturbed scenario. This paper presented a method to calculate the extent of the DRZ surrounding a WIPP disposal room using a WIPP-specific dilatant damage criterion. The constant *C* in the damage criterion was determined by calibrating ultrasonic wave velocity field measurements, obtained in the S-90 drift, to a finite element model that predicts the salt's behavior over time. The results yielded a *C* value of 0.19, which represents the best estimate of the actual field value as it is based on a large number of controlled in situ measurements. When this *C* value is applied, the analysis predicts a maximum DRZ extent of 4.75 m above and 2.25 m below a WIPP disposal room. This upper limit is less than half the extent (about 12 m) currently modeled in WIPP performance assessment; however, the predicted extent below a room is about the same as what is currently modeled.

Several lines of evidence were presented to suggest that ultrasonic velocity measurements are a useful method for assessing damage. (1) In situ gas permeability measurements suggest C = 0.20. (2) A comparative study of microstructural features of damaged core and gas permeability measurements suggest C = 0.18. (3) Laboratory triaxial testing of various bedded rock salts in compression and extension yielded an average calibrated damage factor in the linear damage criterion of C = 0.20.

Further analyses are underway to strengthen these preliminary results. However, the range of *C* values from all lines of evidence yield a much smaller DRZ than is presently used in the WIPP repository performance assessment models.

ACKNOWLEDGEMENTS

This research is funded by WIPP programs administered by the Office of Environmental Management of the United States Department of Energy. Sandia is a multiprogram laboratory operated by Sandia Corporation, a Lockheed Martin Company, for the United States Department of Energy's National Nuclear Security Administration under Contract DE-AC04-94AL85000.

REFERENCES

1. Hansen, F.D. 2003. *The Disturbed Rock Zone at the Waste Isolation Pilot Plant.* SAND2003-3407. Albuquerque, NM: Sandia National Laboratories.
2. Holcomb, D.J. and R.D. Hardy. 2001 Assessing the disturbed rock Zone (DRZ) at the WIPP (Waste Isolation Pilot Plant) in salt using ultrasonic waves. In *Proceedings of the 38th U.S. Rock Mechanics Symposium, 2001*. Eds. D. Elsworthet al. pp. 489-496. Rotterdam: Balkema
3. Brodsky, N.S. 1995 *Thermomechanical damage recovery parameters for rock salt from the Waste Isolation Pilot Plant.* SAND93-7111. Albuquerque, NM: Sandia National Laboratories.
4. Van Sambeek, L.L., J.L Ratigan, and F.D. Hansen. 1993. Dilatancy of rock salt in laboratory tests. In *Proceedings 34th U.S. Symposium on Rock Mechanics*, Madison, WI, 27-30 June 2001. Ed. B.C. Haimson. pp. 245-248. *International Journal of Rock Mechanics and Mining Sciences & Geomechanics Abstracts* 30: 735–738.
5. Park, B. Y., A. E. Ismail, D. J. Holcomb, and C. G. Herrick. 2007. Analysis report for prediction of the extent and permeability of the disturbed rock zone around a WIPP disposal room. ERMS 546370. Carlsbad, NM: Sandia National Laboratories.
6. Munson, D. E., A. F. Fossum, and P. E. Senseny. 1989. Advances in resolution of discrepancies between predicted and measured in situ room closures.

SAND88-2948. Albuquerque, NM: Sandia National Laboratories.

7. Park, B.Y. and J.F. Holland. 2007. *Structural evaluation of WIPP disposal room raised to Clay Seam G*. SAND2007-3334. Albuquerque, NM: Sandia National Laboratories,

8. Stormont, J.C. 1997. In situ gas permeability measurements to delineate damage in rock salt. *Int. J. Rock Mech. Min. Sci.* 34:1055-1064.

9. Bryan, C.R., D.W. Powers, D.M. Chapin, and F.D. Hansen. 2003. Observational studies of halite salt cores extracted from a disturbed rock zone/excavation damage zone at the Waste Isolation Pilot Plant. In *The 2002 International EDZ Workshop: The Excavation Zone – Causes and Effects*. Toronto, Canada, 6 July 2002. Ed J.B. Martino. Report No: 06819-REP-01200-10105-R00. Attachment 1, paper 3. Atomic Energy of Canada Limited.

10. DeVries, K.L., K.D. Mellegard, and G.D. Callahan. 2003. Laboratory testing in support of a bedded salt failure criterion. In *Solution Mining Research Institute Fall Meeting*, Chester, United Kingdom, 5-8 October 2003. pp. 90–113.